Applied Thermal Engineering 115 (2017) 1277–1286

Contents lists available at ScienceDirect

Applied Thermal Engineering

journal homepage: www.elsevier.com/locate/apthermeng

Research Paper

Numerical predictions of thermal conductivities for the silica aerogel and its composites

Wen-Zhen Fang, Hu Zhang, Li Chen, Wen-Quan Tao *

Key Laboratory of Thermo-Fluid Science and Engineering of MOE, School of Energy and Power Engineering, Xi'an Jiaotong University, Xi'an, Shaanxi 710049, China

ARTICLE INFO

Article history:
Received 2 February 2016
Revised 8 September 2016
Accepted 29 October 2016
Available online 31 October 2016

Keywords:
Silica aerogel
Effective thermal conductivity
Discrete ordinate method
Lattice Boltzmann method
Thermal contact resistance

ABSTRACT

In the present paper, two kinds of microstructures are reconstructed for silica aerogels by diffusion-limited cluster-cluster aggregation (DLCA) method and open-cell structure generation method. The discrete ordinate method is adopted to solve radiative transfer equation, and the lattice Boltzmann method (LBM) is adopted to solve the conduction-radiation equation to predict the effective thermal conductivity considering the combined contribution of conduction and radiation. The partial bounce back scheme for thermal LBM is extended to consider the thermal contact resistance between two contact components with different thermal conductivity in aerogels. To validate the accuracy of the present model, some corresponding experimental measurements based on Hot Disk method are conducted. The results show that: the open-cell structure is more suitable for the real aerogel microstructure than DLCA structure; the effective thermal conductivity of the pure aerogel increases rapidly with temperature and is greatly suppressed if additives are doped; the Rosseland equation will over-predict the effective thermal conductivity of pure aerogels, especially at high temperature, but it can be applied for aerogel composites if the optical thickness assumption is satisfied; the thermal contact resistance in aerogels has a significant influence on their effective thermal conductivity, and a larger thermal contact resistance leads to a smaller effective thermal conductivity.

1. Introduction

Silica aerogels are the typical nano-porous insulation materials with high porosity, low density and extremely complicated structure. The pure aerogel is brittle and almost transparent to the wavelength of 2–8 μm, and in practical application, some additives (fibers and opacifiers) are adopted to enhance their mechanical strength and extinction effect [1]. Much attention has been focused on the estimation of the thermal conductivity of silica aerogels. In general, the calculation models can be divided into three categories: theoretical model [2–4], experimental measurement [5–7] and numerical method [8,9]. The effective thermal conductivity of materials is closely associated with their microstructure, and a proper reconstruction structure is required for the numerical method. In the present paper, two different reconstruction methods, diffusion-limited cluster-cluster aggregation (DLCA) method [10,11] and random generation growth method for open-cell (net-like) structure [12], are adopted to regenerate the microstructure of the silica aerogel. Meanwhile, the Hot Disk method is adopted to measure the effective thermal conductivity of the silica aerogel, and to decide which reconstruction method is more suitable for the silica aerogel.

Radiation is the major contribution part of the effective thermal conductivity of the silica aerogels at high temperature. Although many researches have considered the influence of the radiation on the effective thermal conductivity of the silica aerogel, they assumed that the aerogels are optical thickness materials and solved the Rosseland equation rather than the radiative transfer equation [3,6,7]. Mendes et al. [13] pointed out that Rosseland equation can only be applied for the optical thickness of materials larger than 10. However, as for pure aerogel, especially at high temperature, the optical thickness larger than 10 is not satisfied. In addition, the discrete ordinate method (DOM) [14] is adopted to solve the radiative transfer equation, and the lattice Boltzmann method (LBM) is used to solve the energy transport equation with the volumetric radiative source term obtained by solving the radiative transfer equation [15]. In the present paper, the spectral extinction coefficients of fibers and opacifiers are calculated by Mie theory [16] rather than measured by Fourier transform infrared spectrometer [17].

* Corresponding author.
E-mail address: wqtao@mail.xjtu.edu.cn (W.-Q. Tao).

http://dx.doi.org/10.1016/j.applthermaleng.2016.10.184
1359-4311/

In analyzing the effective thermal conductivity of the engineering composite materials, the thermal contact resistance at the interfaces are generally assumed negligible [18]. However, as for aerogels, the negligible thermal contact resistance may overestimate the effective thermal conductivity of the materials. Fig. 1(a) [19] and (b) show the microstructure of the aerogels at the nanoscale level and microscale level, respectively. The solid skeleton of the aerogel is made up of the aggregating nanoparticles. How the nanoparticles aggregate to be a skeleton chain and whether the neighboring nanoparticles contact well will significantly influence the effective thermal conductivity of the aerogels. Furthermore, the thermal contact resistance between the aerogel matrix and additives will also have effects on the effective thermal conductivity. Among the previous studies, a partial bounce-back scheme for thermal LBM was first proposed by Han et al. [20] to consider the thermal contact resistance at the interface and then further developed by Xie et al. [21]. However, those proposed methods are only suitable for the case that the thermal conductivities of the two components adjacent to the interfaces are the same. In the present paper, we will extend this partial bounce-back scheme to be applied for the case that the thermal conductivities of the two components adjacent to the interfaces are different.

This paper is organized as follows. In Section 2, the LBM for conduction-radiation energy transport equation, the DOM for radiative transfer equation and the partial bounce back scheme for considering the thermal contact resistance are presented. In Section 3, the reconstruction method for aerogels, Mie theory for extinction coefficient and Hot Disk method for determining the effective thermal conductivity of aerogels are introduced. In Section 4, the developed numerical method is adopted to predict the effective thermal conductivities of aerogels. Finally, three conclusions are drawn in Section 5.

2. Numerical method

The energy transport equation considering the volumetric radiative heat transfer (conduction-radiation energy transport equation) can be described as:

$$\frac{\partial T}{\partial t} = \left(\frac{\lambda}{\rho c_p}\right)\nabla^2 T - \frac{1}{(\rho c_p)}\nabla \cdot \vec{q}_R \tag{1}$$

where T denotes the temperature; λ is the thermal conductivity; ρc_p is the volume specific capacity; and $\vec{q}_R$ is the radiative heat flux. The calculation speed of the radiative transfer equation is much slower than that of the diffusion equation because two additional angle parameters are involved to fully describe the radiation at any position in 3D space. To reduce calculation time, the thermal radiation is assumed to be transferred only along z direction by neglecting the temperature difference in x-y plane because other side surfaces are assigned to be adiabatic. Mendes et al. [13] found that the results of simplified homogeneous model (1D model) agree well with those of detailed model (3D model) when predicting the effective thermal conductivity of open-cell foams. The detailed model adopted the blocked-off region approach [22] to obtain divergence of 3D radiative heat flux in complex open-cell foam structure, and then solve Eq. (1) to obtain the combined conduction-radiation effective thermal conductivity of the 3D heterogeneous open-cell foams. On the other hand, the simplified homogeneous model solves the 1D conduction-radiation energy transport equation:

$$\frac{\partial T}{\partial t} = \left(\frac{\lambda_{\mathrm{eff,c}}}{\rho c_p}\right)\frac{\partial^2 T}{\partial^2 x} - \frac{1}{(\rho c_p)}\frac{\partial \vec{q}_R}{\partial x} \tag{2}$$

where $\lambda_{\mathrm{eff,c}}$ is the effective conductive thermal conductivity of the 3D heterogeneous conduction. In the present paper, we follow ideas of the simplified homogeneous model. First, the LBM is used to obtain the effective conductive thermal conductivity of the 3D heterogeneous conduction, $\lambda_{\mathrm{eff,c}}$, by solving the 3D pure conduction energy equation. Second, the DOM is adopted to obtain $\partial \vec{q}_R/\partial x$ by solving the 1D radiative transfer equation. Finally, we use the LBM to obtain the total heat flux (combined conductive and radiative heat flux) by solving Eq. (2), and then obtain the combined conduction-radiation effective thermal conductivity.

2.1. The LBM for 3D heterogeneous conduction

To obtain the value of $\lambda_{\mathrm{eff,c}}$, we should solve the pure conduction equation in 3D heterogeneous material:

$$\begin{aligned}\frac{\partial T_A}{\partial t} &= \left(\frac{\lambda}{\rho c_p}\right)_A \nabla^2 T \\ \frac{\partial T_B}{\partial t} &= \left(\frac{\lambda}{\rho c_p}\right)_B \nabla^2 T\end{aligned} \tag{3}$$

where subscripts A and B represent different components. Instead of solving the partial differential equation Eq. (3) directly, in the LBM, the evolution equations for temperature distribution functions are solved on lattices [23–25]. For each component, the evolution of temperature distribution function is [26]:

$$f_i(\vec{r} + \vec{e}_i\Delta t, t + \Delta t) = f_i(\vec{r}, t) - \frac{\Delta t}{\tau}[f_i(\vec{r}, t) - f_i^{eq}(\vec{r}, t)] \tag{4}$$

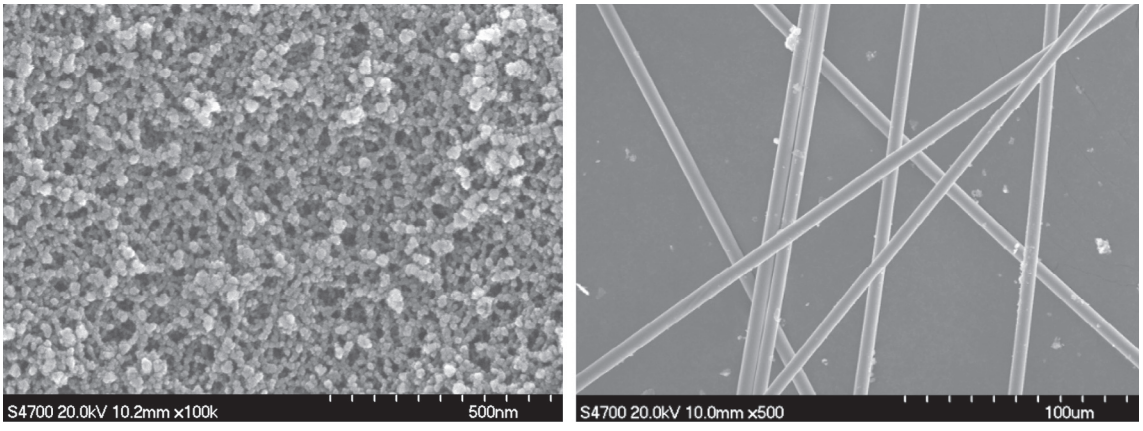

(a) Nanoscale level [19] (b) Microscale level

Fig. 1. Scanning electron microscope pictures of the aerogel and its composites.

where $\vec{r}$ denotes the particle position; t is the real time; Δt is the time step; f_i is the temperature distribution function; and f_i^{eq} is the equivalent distribution function. For the energy governing equation, the D3Q19 model can be reduced to D3Q7 model without loss of accuracy [25]. To save the computational time, we adopt the D3Q7 model. The equivalent distribution function is defined as:

$$f_i^{eq} = \frac{T}{7}, \qquad i = 0-6 \tag{5}$$

In Eq. (4), $\vec{e}_i$ is the discrete velocity [26]:

$$\vec{e}_i = \begin{bmatrix} 0 & 1 & -1 & 0 & 0 & 0 & 0 \\ 0 & 0 & 0 & 1 & -1 & 0 & 0 \\ 0 & 0 & 0 & 0 & 0 & 1 & -1 \end{bmatrix} c \tag{6}$$

For each component in heterogeneous materials, the relations between the relaxation time coefficients and thermal conductivities can be obtained by Chapman-Enskog expansion [26]:

$$\begin{aligned} \tau_A &= \frac{7}{2}\frac{\lambda_A}{(\rho c_p)_A}\frac{1}{c^2\Delta t} + 0.5, \\ \tau_B &= \frac{7}{2}\frac{\lambda_B}{(\rho c_p)_B}\frac{1}{c^2\Delta t} + 0.5 \end{aligned} \tag{7}$$

where c is the lattice speed, and its value should be taken to ensure the value of τ within (0.5, 2) [26].

The local macroscopic temperature can be obtained by:

$$T = \sum_{i=0}^{6} f_i \tag{8}$$

With the half lattice division treatment [27] for the interface, we should only set [29]:

$$(\rho c_p)_A = (\rho c_p)_B = \rho c_p \tag{9}$$

to ensure the heat flux continuity at the interface. The local conductive heat flux along z direction can be obtained by [26]:

$$q_{c,z} = -\rho c_p \left(\sum_i e_{i,z} f_i \right) \frac{\tau - 0.5}{\tau} \tag{10}$$

Then,

$$\lambda_{\text{eff},c} = \frac{\int q_{c,z} dA}{A\Delta T / L} \tag{11}$$

For the 3D cubic unit cell structure, two opposite boundary surfaces along the z direction are set to be isothermal but at different temperatures, and other surfaces are set to be adiabatic. For the details of boundary condition treatments in the LBM, one can refer to references [26,28].

2.1.1. Negligible thermal contact resistance (TCR) at the interface

If there is no TCR at the interface between two different components, the continuity of the temperature and heat flux at the interface should be satisfied. In the present paper, the interface is placed at the middle of the lattice nodes. With the assumption of the equality of ρc_p for different components, the continuity of temperature and heat flux can be ensured.

2.1.2. Non-negligible thermal contact resistance (TCR) at the interface

If the TCR at the interface is non-negligible, the heat flux should also be continuous but temperature will have a drop at the interface. To consider the TCR at the interface for thermal LBM, a partial bounce-back scheme [20,21] was proposed. However, previous methods are only suitable for the case that the thermal conductivities of two components adjacent to the interface should be the same. In the present paper, we will extend this partial bounce-back scheme for the case that the thermal conductivities of components adjacent to the interface can be different. The idea of the partial bounce-back scheme is introducing a parameter δ within (0,1) to represent the portion that temperature distribution functions bounces back from the interface when they try to stream through the interface (as shown in Fig. 2, D3Q7 model):

$$f_5^I = \delta f_6^I + (1-\delta) f_5^I \tag{12}$$

where

$$\begin{aligned} f_6^I &= f_6^I - \frac{1}{\tau_I}\left(f_6^I - \frac{T^I}{7}\right) \\ f_5^J &= f_5^J - \frac{1}{\tau_J}\left(f_5^J - \frac{T^J}{7}\right) \end{aligned} \tag{13}$$

are the post-collision temperature distribution functions.

To obtain the relation between δ and the TCR, we consider a 1D heat conduction problem. Then, the TCR at the interface can be obtained by the subtraction of the total thermal resistance between nodes I and J and the per lattice grid thermal resistance:

$$R_c = R_T - R_g \tag{14}$$

and

$$R_g = \frac{\Delta z/2}{\lambda_I} + \frac{\Delta z/2}{\lambda_J} = \frac{7}{4c\rho c_p}\left(\frac{1}{\tau_I - 0.5} + \frac{1}{\tau_J - 0.5}\right) \tag{15}$$

If the heat conduction reaches the steady state, the following relations will be satisfied if the equivalent distribution function is defined by Eq. (5) [21].

$$f_0 = f_0^{eq} = \frac{T}{7},\ f_1 = f_3 = f_1^{eq} = \frac{T}{7},\ f_2 = f_4 = f_2^{eq} = \frac{T}{7} \tag{16}$$

From Eqs. (10) and (16), we have:

$$q_z = \rho c_p \left(f_6^I - f_5^I\right) c \frac{\tau_I - 0.5}{\tau_I} = \rho c_p \left(f_6^J - f_5^J\right) c \frac{\tau_J - 0.5}{\tau_J} \tag{17}$$

$$\begin{cases} \frac{2}{7}T^I = f_5^I + f_6^I \\ \frac{2}{7}T^J = f_5^J + f_6^J \end{cases} \tag{18}$$

Combining Eqs. (17) and (18) yields:

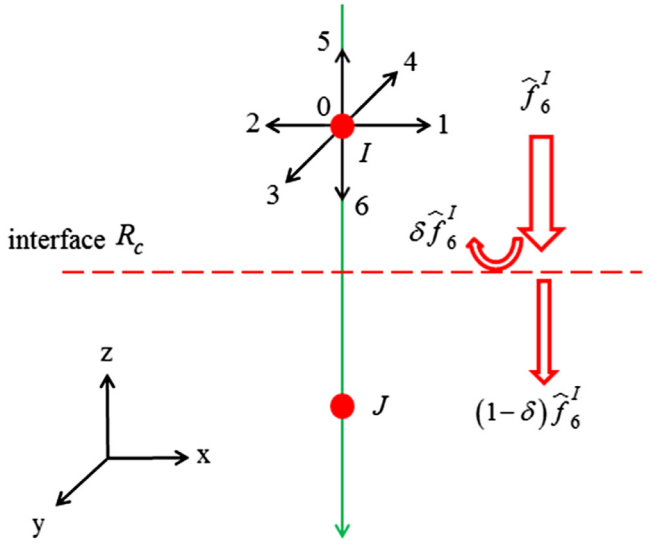

Fig. 2. Partial bounce-back scheme.

$$\begin{cases} f_6^I = \frac{T^I}{7} + \frac{q_z}{2c\rho c_p}\frac{\tau_I}{\tau_I - 0.5} & (a) \\ f_5^I = \frac{T^I}{7} - \frac{q_z}{2c\rho c_p}\frac{\tau_I}{\tau_I - 0.5} & (b) \end{cases} \tag{19}$$

and

$$\begin{cases} f_6^J = \frac{T^J}{7} + \frac{q_z}{2c\rho c_p}\frac{\tau_J}{\tau_J - 0.5} & (a) \\ f_5^J = \frac{T^J}{7} - \frac{q_z}{2c\rho c_p}\frac{\tau_J}{\tau_J - 0.5} & (b) \end{cases} \tag{20}$$

Substituting Eqs. (13), (19.a) and (20.b) into the Eq. (12) yields:

$$f_5^I = \delta\left[\frac{T^I}{7} + \frac{q_z}{2c\rho c_p}\frac{\tau_I - 1}{\tau_I - 0.5}\right] + (1-\delta)\left[\frac{T^J}{7} - \frac{q_z}{2c\rho c_p}\frac{\tau_J - 1}{\tau_J - 0.5}\right] \tag{21}$$

Combining Eqs. (19.b) and (21), we have

$$q_z = \frac{2}{7}\rho c_p c(1-\delta)(T^I - T^J)\Big/\left[\left(\frac{0.5}{\tau_I - 0.5} + \frac{0.5}{\tau_J - 0.5}\right)(1-\delta) + 2\delta\right] \tag{22}$$

The total thermal resistance is:

$$R_T = \frac{(T^I - T^J)}{q_z} = \frac{7}{2\rho c_p c}\left(\frac{0.5}{\tau_I - 0.5} + \frac{0.5}{\tau_J - 0.5}\right) + \frac{7\delta}{\rho c_p c(1-\delta)} \tag{23}$$

Finally, we can obtain the relation between TCR and δ:

$$R_c = R_T - R_g = \frac{7\delta}{\rho c_p c(1-\delta)} \tag{24}$$

2.2. The discrete ordinate method (DOM) for radiative transfer equation

For the absorbing, emitting and scattering medium, the radiative transfer equation in any direction s can be described as [29,30]:

$$\frac{dI(\vec{r},\vec{s})}{ds} = -\beta I(\vec{r},\vec{s}) + \beta S \tag{25}$$

where I is the intensity, β is the extinction coefficient, and S is the source term given by:

$$S = (1-\omega)I_b(\vec{r}) + \frac{\omega}{4\pi}\int_{\Omega'=4\pi} I(\vec{r},\vec{s})\Phi(\vec{r},\vec{s}',\vec{s})\mathrm{d}\Omega' \tag{26}$$

where ω is the scattering albedo, $\Phi(\vec{r},\vec{s}',\vec{s})$ is the scattering phase function. If the scattering is assumed to be isotropic, $\Phi(\vec{r},\vec{s}',\vec{s}) = 1$. The source term becomes:

$$\begin{aligned} S &= (1-\omega)I_b(\vec{r}) + \frac{\omega}{4\pi}\int_{\Omega'=4\pi} I(\vec{r},\vec{s})\mathrm{d}\Omega' \\ &= (1-\omega)I_b(\vec{r}) + \frac{\omega}{4\pi}G \end{aligned} \tag{27}$$

where G is the incident radiation. In one-dimensional DOM, the radiative transfer equation for isotropic scattering medium is [31]:

$$\mu^m\frac{\partial I^m}{\partial z} = -\beta I^m + \beta(1-\omega)I_b + \beta\frac{\omega}{4\pi}G \tag{28}$$

where $\mu = \cos\alpha$ is the direction cosine. Integrating Eq. (28) over the control volume cell yields [31]:

$$\mu^m(I_N^m - I_S^m) = -\beta\Delta z I_P^m + \Delta z S_P^m \tag{29}$$

where I_N^m and I_S^m are the intensities at the north and south face of control volume, respectively; I_P^m and S_P^m are the intensity and source term at the center of control volume cell, respectively. A linear relation is chosen for intensities at the same control volume cell [32]:

$$I_P^m = \gamma_z I_N^m + (1-\gamma_z)I_S^m \tag{30}$$

where γ_z is a constant, and $0.5 \leqslant \gamma_z \leqslant 1$. Substituting Eq. (30) into Eq. (29) yields [32]:

$$I_P^m = \begin{cases} \frac{\mu^m I_S^m/\gamma_z + S_P^m\Delta z}{\mu^m/\gamma_z + \beta\Delta z}, & \mu > 0 \\ \frac{|\mu^m| I_N^m/\gamma_z + S_P^m\Delta z}{|\mu^m|/\gamma_z + \beta\Delta z}, & \mu < 0 \end{cases} \tag{31}$$

For the diffuse-gray boundary condition, the unknown boundary intensities can be obtained by [31]:

$$I^m = \frac{\varepsilon\sigma T_b^4}{\pi} + \left(\frac{1-\varepsilon}{\pi}\right)2\pi\sum_{i=1}^{M/2} I^m\cos\ \alpha^m\sin\ \alpha^m\sin\ (\Delta\alpha^m) \tag{32}$$

Once the intensities are obtained, the radiative heat flux can be calculated by [31]:

$$\begin{aligned} q_R &= 2\pi\int_{\alpha=0}^{\pi} I(\alpha)\cos\alpha\sin\alpha\mathrm{d}\alpha \\ &\approx 2\pi\sum_{m=1}^{M} I^m\cos\alpha^m\sin\alpha^m\sin(\Delta\alpha^m) \end{aligned} \tag{33}$$

and the divergence of radiative heat flux required for Eq. (2) can be obtained by [32]:

$$\nabla\cdot\vec{q}_R = \beta(1-\omega)(4\sigma T^4 - G) \tag{34}$$

2.3. The LBM for conduction-radiation energy transport equation

With the $\lambda_{\mathrm{eff,c}}$ obtained from Eq. (11) and the divergence of radiative heat flux obtained from Eq. (34), a D1Q2 LB model is adopted to solve 1D conduction-radiation energy transport equation (Eq. (2)). The evolution equation of the temperature distribution function is shown below [33]

$$f_i(\vec{r}+\vec{e}_i\Delta t, t+\Delta t) = f_i(\vec{r},t) - \frac{\Delta t}{\tau}[f_i(\vec{r},t) - f_i^{eq}(\vec{r},t)] - \frac{\Delta t}{\rho c_p}w_i\frac{\partial\vec{q}_R}{\partial x} \tag{35}$$

Here, $w_i = 1/2$, and [33]

$$\tau = \frac{\lambda_{eff,c}}{(\rho c_p)}\frac{1}{c^2\Delta t} + 0.5 \tag{36}$$

2.4. Validation

The benchmarks of LBM with half lattice division scheme for predicting the effective thermal conductivity of heterogeneous materials [26,34], the LBM for conduction-radiation energy transport equation [33] and the DOM for solving the radiative transport equation [14] have been done in previous studies. To reduce the length of this paper, their benchmark validations will not be shown again. Here, only benchmarks of the partial bounce back scheme for considering the TCR at the interface between two different thermal conductivity components will be presented.

Consider a 3D pure conduction process through two contact solid materials of different thermal conductivities with TCR at the interface. Fig. 3(a) shows the schematic of the case (a cross section of 3D cubic). The volumetric specific capacity of two components, ρc_p, is chosen to be unity. The temperature distributions along the centerline of 3D cubic for different δ are shown in Fig. 3(b). The theoretical solution of temperature drop at the interface and effective thermal conductivity of this composite material are:

$$\Delta T = \frac{R_c}{\frac{N-1}{2}\frac{\Delta z}{\lambda_1} + R_c + \frac{N-1}{2}\frac{\Delta z}{\lambda_2}} \tag{37}$$

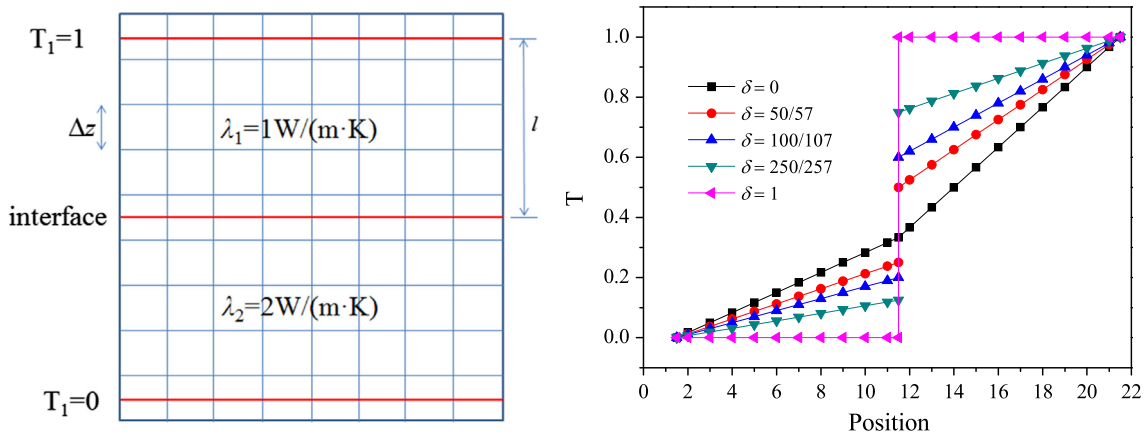

(a) Schematic of case (cross section) (b) Temperature distributions along centerline

Fig. 3. Validation of partial bounce back scheme.

$$\lambda_e = \frac{2l}{\frac{l}{\lambda_1} + R_c + \frac{l}{\lambda_2}} \tag{38}$$

where N is the number of lattice nodes and R_c is obtained from Eq. (24). The grid independence of this case has been checked, and it is found that $N = 21$ is enough. The accuracy of the partial bounce back scheme is validated by the good agreement of theoretical and numerical results shown in Table 1.

3. Application for silica aerogel and its composites

3.1. The reconstruction method

Silica aerogel is reported to be the open-cell (netlike) porous material prepared by the sol-gel process [2]. To properly describe how nanoparticles aggregate together, two reconstruction methods are adopted to reproduce the aerogels (at nanoscale level). One is the diffusion-limited cluster-cluster aggregation (DLCA) method [10,11], the other is the random generation growth method for the open-cell porous material [12] (hereafter called open-cell method). The DLCA method is widely used to reconstruct the microstructures that are prepared by the sol-gel technique, while the open-cell method is suitable for the open-cell porous material which can ensure the solid skeleton of the material to be continuous. The reconstructed unit cell structures based on DLCA method and open-cell method are shown in Fig. 4(a) and (b), respectively. Their grid numbers are all $100 \times 100 \times 100$, and each grid step is 4 nm. In the present paper, the numerical predictions of conductive thermal conductivities of aerogels, $\lambda_{eff,c}$, are obtained based on these two reconstruction methods. As for aerogel composites doped with fibers and opacifiers, the reconstructed unit cell structure is shown in Fig. 5 (at microscale level). The matrix (white part in Fig. 5) is the pure aerogel. The grid number is $100 \times 100 \times 100$, and each grid step is 2 μm. As shown in Fig. 5, the opacifiers are assumed to be spherical and randomly distributed in space, while the fibers are assumed to be randomly distributed in the plane vertical to the heat flux direction.

3.2. Mie theory for obtaining the extinction coefficient of aerogel composites

Aerogel composites are doped with fibers and opacifiers to enhance their extinction effects, and therefore reduce the radiative heat flux at high temperature. If opacifiers are assumed to be spherical, Mie theory can be applied to calculate the spectral extinction coefficient of opacifiers [35]:

$$Q_{ext} = \frac{2}{x^2} Re\left[\sum_{n=1}^{\infty}(2n+1)(a_n + b_n)\right] \tag{39}$$

$$\beta_{e\lambda,op} = \frac{3}{2} Q_{ext} \frac{\phi_{op}}{D_{op}} \tag{40}$$

If fibers are assumed to be infinite long and randomly distributed in the plane vertical to the heat flux direction, the spectral extinction coefficient of fibers can be calculated by [3]:

$$Q_{ext}(\xi) = \frac{1}{x}\left[Re\left(b_{0I} + 2\sum_{n=1}^{\infty} b_{nI}\right) + Re\left(a_{0II} + 2\sum_{n=1}^{\infty} a_{nII}\right)\right] \tag{41}$$

$$\beta_{e\lambda,f} = \frac{4\phi_f}{\pi D_f} Q_{ext} \tag{42}$$

For more details of Mie theory, one can see reference [16].

The mean extinction coefficient of aerogel composites can be obtained by [3]:

$$\frac{1}{\beta_T} = \int_0^{\infty} \frac{1}{\beta_{e\lambda}} \frac{\partial E_{b\lambda}}{\partial E_b} d\lambda \tag{43}$$

Table 1
Comparisons of theoretical solution and simulation results.

δ	R_c	ΔT			λ_e/(W m^{-1} K^{-1})		
	m^2 K W^{-1}	Theoretical	Numerical	Deviation	Theoretical	Numerical	Deviation
0	0	0	0	0	1.3333	1.3333	0
50/57	0.05	0.2500	0.2501	0.04%	1.0000	0.9999	−0.01%
100/107	0.1	0.4000	0.3999	−0.025%	0.8000	0.8001	0.0125%
250/257	0.25	0.6250	0.6250	0	0.5000	0.5000	0
1	Infinity	1.0000	1.0000	0	0	0	0

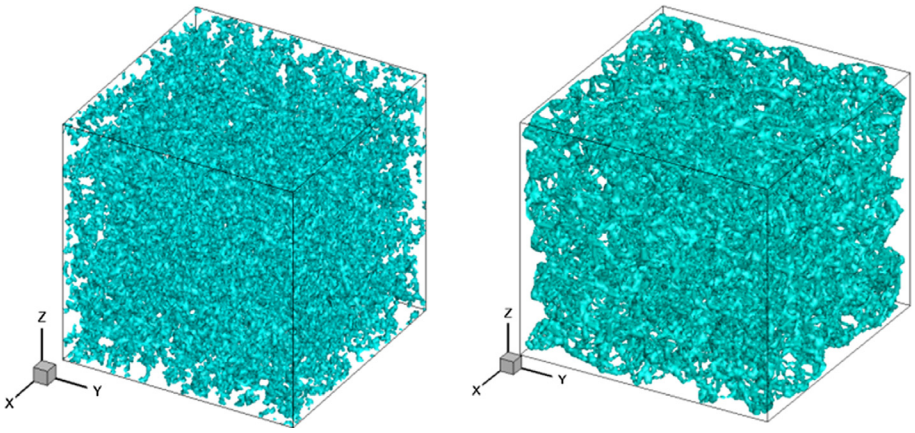

(a) DLCA structure (b) Open-cell structure

Fig. 4. Reconstructed unit cell for pure aerogel.

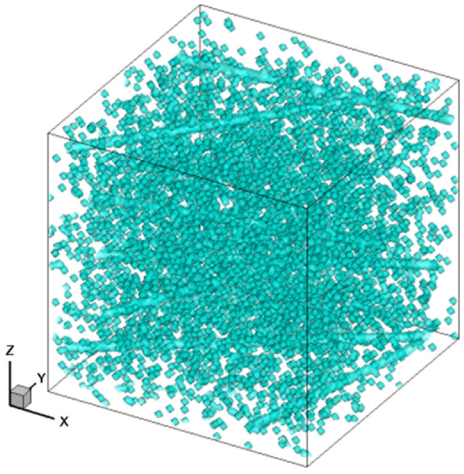

Fig. 5. Reconstructed unit cell of the aerogel composites.

$$\beta_{e\lambda} = \beta_{e\lambda,a} + \beta_{e\lambda,op} + \beta_{e\lambda,f} \tag{44}$$

where $\beta_{e\lambda,a}$, $\beta_{e\lambda,op}$, $\beta_{e\lambda,f}$ are the spectral extinction coefficients of pure aerogels, opacifiers and fibers, respectively. In the present paper, the spectral extinction coefficient of the pure aerogel is obtained from reference [36], while the spectral extinction coefficients of fibers and opacifiers are obtained according to Mie theory.

3.3. The thermal conductivity of components in aerogels

To determine the effective thermal conductivity of the silica aerogel, one should first determine the thermal conductivity of gas and solid in aerogels. The gas thermal conductivity in nanoporous aerogels can be calculated by [37]:

$$\lambda_g = \frac{60.22 \times pT^{-0.5}}{0.25\rho_a S_a/\phi_a + 4.01 \times 10^4 \times pT^{-1}} \tag{45}$$

where p is the pressure; T is the temperature; and S_a is the specific surface area given by [6]:

$$S_s = (324.3/\rho_a + 5.03) \times 10^5 \tag{46}$$

ϕ_a is the porosity, defined as:

$$\phi_a = 1 - \rho_a/\rho_{bulk} \tag{47}$$

where ρ_a is the density of the pure aerogel, and ρ_{bulk} is the bulk density of the silicon dioxide.

The solid thermal conductivity of the bulk silicon dioxide can be obtained by [3]:

$$\lambda_{bulk} = 0.7526 + 3.1286 \times 10^{-3}T - 4.5242 \times 10^{-6}T^2 + 3.525 \times 10^{-9}T^3 \tag{48}$$

The size of solid particle is of the same order as the phonon mean free path, and therefore the nanoscale size effect on the thermal conductivity should be considered [8]:

$$\lambda_s = \frac{3a}{3a + 8l}\lambda_{bulk} \tag{49}$$

where a is the size of the solid particle, and l is the phonon mean free path.

The fiber is made of the silicon dioxide, and its thermal conductivity is shown in Eq. (48). As for opacifiers (SiC) in aerogel composites, their thermal conductivities variation with temperature can be obtained from reference [38].

3.4. Thermal conductivity measurement for aerogels and its composites

In the present paper, a thermal constants analyser (Hot Disk TPS 2500s) [39,40] is adopted to measure the effective thermal conductivity of aerogels and their composites. During the measurement, Hot Disk probe operates as the heat source as well as the temperature sensor. The Hot Disk probe should be placed between two identical specimen halves. A heat pulse is then supplied by the probe to generate a dynamic temperature field within specimens. The temperature increment of the Hot Disk probe surface facing specimens depends on the thermal properties of specimens, and it can be expressed as [40]:

$$\Delta T(\tau) = \frac{P_0}{\pi^{3/2} r \lambda} D(\tau) \tag{50}$$

After dealing with the record temperature increase curve, one can determine the thermal conductivity and thermal diffusivity of the specimen simultaneously.

The effective thermal conductivities of aerogel and aerogel composites are measured at different gas pressure and temperature. We put the specimens in a tube heating furnace in which temperature can be adjusted from room temperature to 1000 K and pressure can be controlled from 0.01 Pa to 1 MPa by a connected molecular vacuum pump and high pressure gas source.

4. Results and discussion

To solve Eq. (2), we need some input parameters, such as the conductive thermal conductivity of 3D heterogeneous conduction $\lambda_{\text{eff,c}}$, extinction coefficient β and the divergence of radiative heat flux $\nabla \cdot \vec{q}_R$. Mie theory is adopted to obtain the extinction coefficient of aerogels and their composites. LBM is adopted to obtain the conductive thermal conductivity of 3D heterogeneous conduction $\lambda_{\text{eff,c}}$. DOM is adopted to obtain the radiative heat flux and its divergence $\nabla \cdot \vec{q}_R$. Once the temperature field is converged, the effective thermal conductivity of the aerogels and their composites can be obtained by:

$$\lambda_e = q_t L/\Delta T = (q_c + q_r)L/\Delta T \tag{51}$$

where q_t is the total heat flux of conduction and radiation, and ΔT is the temperature difference. The flowchart of the numerical procedures is presented in Fig. 6. The simulations were performed at the high performance computer at the Key Laboratory of Thermo-Fluid Science & Engineering of MOE of Xi'an Jiaotong University. The CPU is the Intel Xeon E5-2680 V2, and the typical running time for a single case is about 8 h.

4.1. Comparison with experimental data

The numerical predictions of the total effective thermal conductivity of aerogels based on two kinds of reconstructed unit cell structures are compared with experimental data measured by Hot Disk method, as shown in Fig. 7. It can be seen that the numerical predictions based on the open-cell (netlike) structure agree more well with experimental data than those based on the DLCA structure. At ambient temperature, the thermal radiation through aerogels can be neglected, and therefore the effective thermal conductivity of aerogels depends on the heat transfer quantity through the solid skeleton when the gas pressure approaches zero. Although both reconstructed structures can ensure the nanoparticles aggregating to be continuously connected chains, their heat transfer channels numbers are much different. For DLCA method,

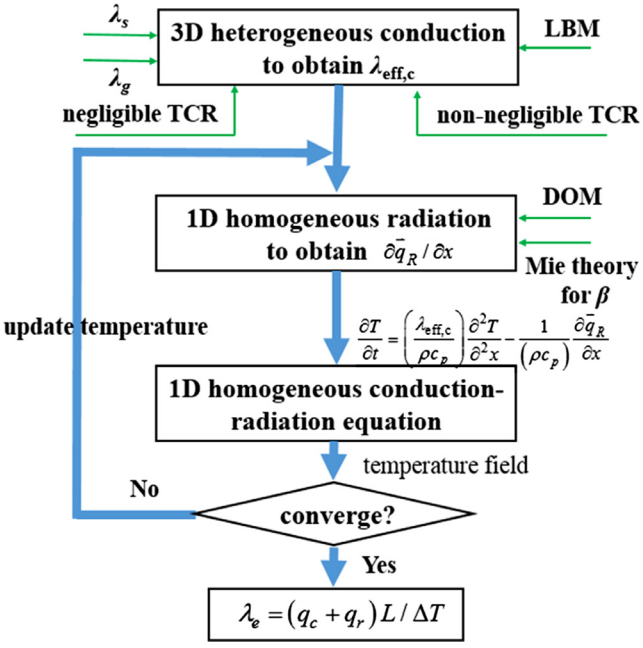

Fig. 6. Flowchart of numerical procedures.

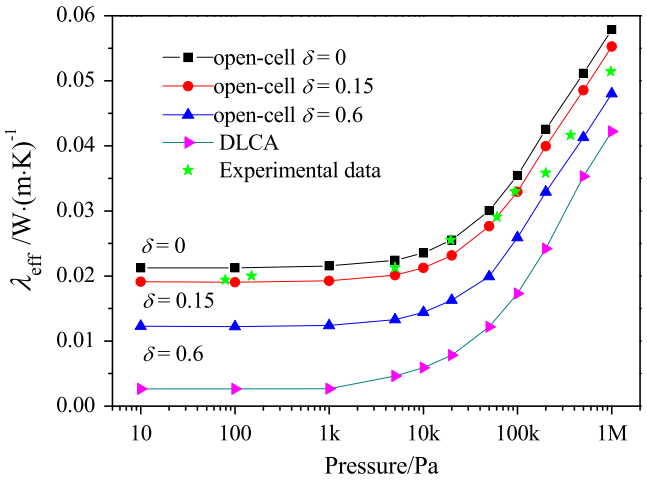

Fig. 7. Comparisons of effective thermal conductivity between numerical results and experimental data.

there only exists one cluster when the reconstruction process is over. It means that heat flux path from top to bottom through the solid skeleton is only single channel and extremely long. As for the reconstructed structure obtained by open-cell method, there exists lots of continuous solid skeleton chains from top to bottom along the heat transfer direction. As a result, the numerical predictions of effective thermal conductivities at low pressure based on the DLCA structure almost approach zero while those obtained based on the open-cell method approach a certain value. The open-cell microstructure is more suitable for the real structure of aerogels in the present study, and it well simulates the aggregating process of the neighboring nanoparticles linking to be particle-particle contact chains. Furthermore, we adopt the partial bounce-back scheme to mimick the TCR between the nanoparticles of the open-cell microstructure. The numerical results of open-cell structure with $\delta = 0$, $\delta = 0.15$ and $\delta = 0.60$ are shown in Fig. 7. δ represents the portion bounces back from the interface of two contact nanoparticles. Here, $\delta = 0.15$ represents $R_c = 1.372 \times 10^{-9}$ m^2 K W^{-1}, and $\delta = 0.6$ represents $R_c = 1.167 \times 10^{-8}$ m^2 K W^{-1}. It can be seen that a lager TCR between two aggregating nanoparticles will lead to a smaller effective thermal conductivity, and the numerical results with $\delta = 0.15$ have a better agreement with experimental data than those obtained with $\delta = 0$ and $\delta = 0.6$. We suppose that the aerogels made by the same manufacturing process have the similar microstructures, and therefore choose $\delta = 0.15$ for other samples. It is found that using $\delta = 0.15$ to determine the effective thermal conductivity of the aerogel composites also fits the experimental data well (see Fig. 9(b)).

4.2. The effect of temperature on pure aerogels

The variations of the effective thermal conductivity of pure aerogels with temperature at the density of 114 kg/m^3 and 185 kg/m^3 are shown in Figs. 8(a) and (b), respectively. Based on the optical thickness assumption, the Rosseland equation [6]

$$\lambda_r = \frac{16}{3\beta}\sigma T^3 \tag{52}$$

is widely used to obtain the radiative thermal conductivity of aerogels and aerogel composites, and then the total effective thermal conductivity of aerogels is the summation of the conductive thermal conductivity, $\lambda_{\text{eff,c}}$, and radiative thermal conductivity, λ_r. It can be seen from Fig. 8 that the results obtained by Rosseland equa-

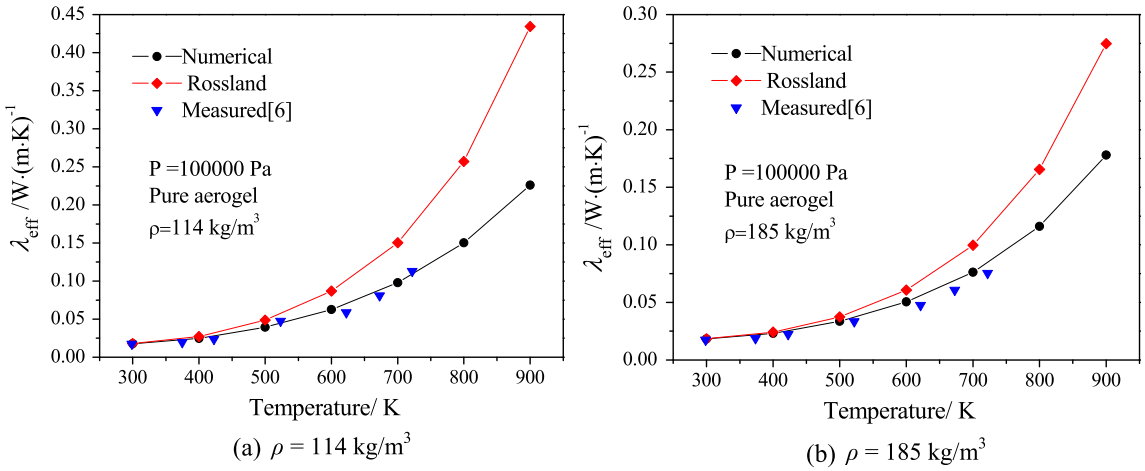

Fig. 8. Variations of effective thermal conductivities with temperature.

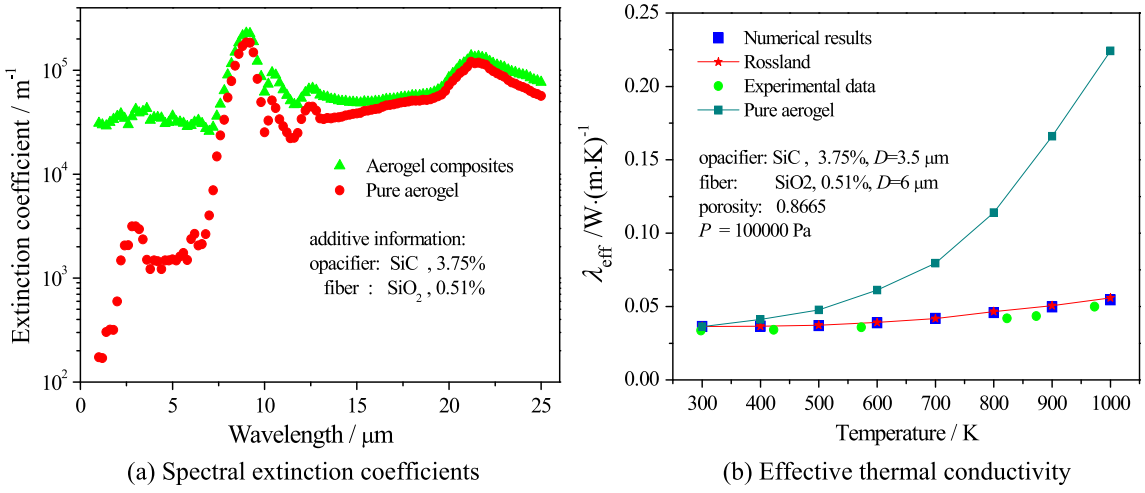

Fig. 9. Effect of additives of aerogel composites on effective thermal conductivity.

tion will over-predict the thermal conductivity, especially at high temperature. It is because the extinction coefficient of pure aerogels, β, is not big enough to satisfy the optical thickness assumption for the Rosseland equation and β decreases rapidly with the increasing temperature. However, the numerical predictions obtained by solving radiative transfer equation agree well with the existing experimental data in the temperature range from 300 K to 723 K [6]. It should be noted that the experimental data in reference [6] did not contain data over 750 K. We can also see that the effective thermal conductivities of pure aerogels increase rapidly when temperature increases, especially at high temperature. It is because the radiation rapidly increases with temperature and even becomes dominant at high temperature. Aerogels with larger density have a larger extinction coefficient and a smaller radiative thermal conductivity. Therefore, the effective thermal conductivity of the pure aerogel with density of 185 kg/m^3 is smaller than that of 114 kg/m^3 at high temperature.

4.3. The effect of doped additives on aerogel composites

Fibers and opacifiers are doped in aerogels to improve the extinction effect of the materials. Comparisons of spectral extinction coefficients between the pure aerogels and their composites are shown in Fig. 9(a). It can be seen that spectral extinction coefficients of aerogels within wavelength of 2–8 μm is greatly improved when additives (fibers and opacifiers) are doped. Therefore, the mean extinction coefficients of aerogel composites are much larger than those of the pure aerogel.

The doped opacifiers and fibers also enhance the heat conduction in aerogels because the thermal conductivities of opacifiers and fibers are larger than those of the aerogel matrix. To consider the effect of additives on the insulation performance of aerogels, the numerical predictions of the effective thermal conductivities of aerogel composites are conducted based on the reconstructed unit cell structure as shown in Fig. 5. Fig. 9(b) shows the comparisons of the total effective thermal conductivities of aerogel composites between experimental data and numerical predictions at different temperature. The experimental data are measured by Hot Disk method. The information of the measured aerogel composites is presented in Fig. 8(b). It can be seen that doped additives can significantly decrease the total effective thermal conductivity of aerogels, especially at high temperature. It is because the doped additives can greatly improve the mean extinction coefficients of aerogel composites and therefore reduce the radiative thermal conductivity at high temperature. In Fig. 9(b), the results obtained by Rosseland equation (Eq. (52)) are compared with numerical results. It can be seen that they fit rather well. The reasons can be attributed to the great improvement of the extinction coefficient and the optical thickness assumption is now satisfied for the Rosseland equation.

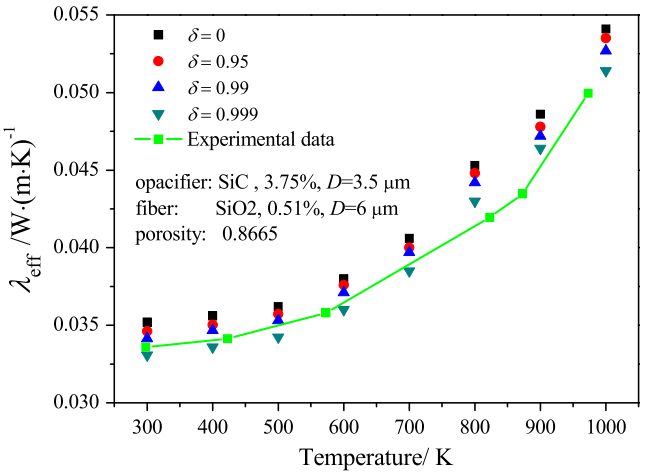

Fig. 10. The effect of TCR on effective thermal conductivity of aerogel composites.

4.4. The effect of thermal contact resistance

The effect of the TCR in the open-cell structure for pure aerogels has been considered in Section 4.1. As shown in Fig. 7, the TCR between contact nanoparticles will have a significant influence on the effective thermal conductivity of pure aerogels. The value of the effective thermal conductivity of pure aerogels with $R_c = 1.167 \times 10^{-8}$ m^2 K W^{-1} ($\delta = 0.60$) between two contact nanoparticles is only 58.8% of those without TCR ($\delta = 0$) at vacuum. As for aerogel composites, the effect of the TCR at the interface of the aerogel matrix and additives are shown in Fig. 10. In this case, $\delta = 0.95$ represents $R_c = 8.867 \times 10^{-7}$ m^2 K W^{-1}; $\delta = 0.99$ represents $R_c = 4.619 \times 10^{-6}$ m^2 K W^{-1}; $\delta = 0.999$ represents $R_c = 4.662 \times 10^{-5}$ m^2 K W^{-1}. The numerical results of $R_c = 4.662 \times 10^{-5}$ m^2 K W^{-1} have a rather good agreements with experimental data, while numerical results without TCR will over-predict the effective thermal conductivity about 6%.

5. Conclusions

In the present paper, the combination of DOM and LBM is adopted to numerically predict the total effective thermal conductivity of aerogels and their composites considering the combined effect of conduction and radiation. Numerical predictions of the total effective thermal conductivity of pure aerogel are based on two kinds of reconstructed microstructure. Meanwhile, the Hot Disk method is adopted to measure the effective thermal conductivity. The influences factors on the effective thermal conductivity of the aerogels and their composites are then investigated. We conclude that:

1. The reconstructed microstructure obtained by random generation growth method for open-cell structure is more suitable for the aerogel structure than that obtained by the diffusion-limited cluster-cluster aggregation method; the effective thermal conductivity of pure aerogels increases rapidly with temperature. If additives (fibers and opacifiers) are doped in aerogels, the effective thermal conductivity of aerogel composites will be greatly impressed, especially at high temperature.
2. Rosseland equation will over-predict the effective thermal conductivity of pure aerogels, especially at high temperature, while it can be applied for aerogel composites if the optical thickness assumption is satisfied;
3. The thermal contact resistance between two contact nanoparticles will have a significant influence on the effective thermal conductivity of the pure aerogel; a larger TCR will lead to a smaller effective thermal conductivity of pure aerogels; as for the aerogel composites, numerical results without TCR will over-predict the effective thermal conductivity about 6%.

Acknowledgement

This research was supported by the Key Project of International Joint Research of National Natural Science Foundation of China (51320105004) and the Key Project of National Natural Science Foundation of China (51136004).

References

[1] J. Fricke, T. Tillotson, Aerogels: production, characterization, and applications, Thin Solid Films 297 (1997) 212–223.
[2] S. Zeng, A. Hunt, R. Greif, Geometric structure and thermal conductivity of porous medium silica aerogel, J. Heat Transfer 117 (1995) 1055–1058.
[3] T. Xie, Y.L. He, Z.J. Hu, Theoretical study on thermal conductivities of silica aerogel composite insulating material, Int. J. Heat Mass Transfer 58 (2013) 540–552.
[4] X. Lu, R. Caps, J. Fricke, C. Alviso, R. Pekala, Correlation between structure and thermal conductivity of organic aerogels, J. Non-Cryst. Solids 188 (1995) 226–234.
[5] E. Cohen, L. Glicksman, Analysis of the transient hot-wire method to measure thermal conductivity of silica aerogel: influence of wire length, and radiation properties, J. Heat Transfer 136 (2014) 041301.
[6] G. Wei, Y. Liu, X. Zhang, F. Yu, X. Du, Thermal conductivities study on silica aerogel and its composite insulation materials, Int. J. Heat Mass Transfer 54 (2011) 2355–2366.
[7] D. Dan, H. Zhang, W.-Q. Tao, Effective structure of aerogels and decomposed contributions of its thermal conductivity, Appl. Therm. Eng. 72 (2014) 2–9.
[8] J.J. Zhao, Y.Y. Duan, X.D. Wang, B.X. Wang, A 3-D numerical heat transfer model for silica aerogels based on the porous secondary nanoparticle aggregate structure, J. Non-Cryst. Solids 358 (2012) 1287–1297.
[9] M. Wang, X. Wang, J. Wang, N. Pan, Grain size effects on effective thermal conductivity of porous materials with internal thermal contact resistance, J. Porous Media 16 (2013).
[10] X. Zhao, Z. Li, H. Liu, W. Tao, The influences of microstructural parameters on the gaseous thermal conductivity in nanoporous material, Proceedings of the 29th International Symposium on Rarefied Gas Dynamics, 1628, AIP Publishing, 2014, pp. 205–211.
[11] A. Rahmani, C. Benoit, R. Jullien, G. Poussigue, A. Sakout, Dynamical properties of a diffusion-limited cluster-cluster aggregation model, J. Phys.-Condens. Matter 8 (1996) 5555.
[12] M. Wang, N. Pan, Modeling and prediction of the effective thermal conductivity of random open-cell porous foams, Int. J. Heat Mass Transfer 51 (2008) 1325–1331.
[13] M.A. Mendes, P. Talukdar, S. Ray, D. Trimis, Detailed and simplified models for evaluation of effective thermal conductivity of open-cell porous foams at high temperatures in presence of thermal radiation, Int. J. Heat Mass Transfer 68 (2014) 612–624.
[14] W. Fiveland, Three-dimensional radiative heat-transfer solutions by the discrete-ordinates method, J. Thermophys. Heat Transfer 2 (1988) 309–316.
[15] S.C. Mishra, H.K. Roy, Solving transient conduction and radiation heat transfer problems using the lattice Boltzmann method and the finite volume method, J. Comput. Phys. 223 (2007) 89–107.
[16] C.F. Bohren, D.R. Huffman, Absorption and Scattering of Light by Small Particles, John Wiley & Sons, 2008.
[17] J. Kuhn, T. Gleissner, M. Arduini-Schuster, S. Korder, J. Fricke, Integration of mineral powders into SiO 2 aerogels, J. Non-Cryst. Solids 186 (1995) 291–295.
[18] M. Wang, N. Pan, Predictions of effective physical properties of complex multiphase materials, Mater. Sci. Eng. R-Rep. 63 (2008) 1–30.
[19] H. Zhang, W. Gu, M.J. Li, W.Z. Fang, Z.Y. Li, W.Q. Tao, Influence of environmental factors on the adsorption capacity and thermal conductivity of silica nano-porous materials, J. Nanosci. Nanotechnol. 15 (2015) 3048–3054.
[20] K. Han, Y. Feng, D. Owen, Modelling of thermal contact resistance within the framework of the thermal lattice Boltzmann method, Int. J. Therm. Sci. 47 (2008) 1276–1283.
[21] C. Xie, J. Wang, D. Wang, N. Pan, M. Wang, Lattice Boltzmann modeling of thermal conduction in composites with thermal contact resistance, Commun. Comput. Phys. 17 (2015) 1037–1055.
[22] P. Talukdar, Discrete transfer method with the concept of blocked-off region for irregular geometries, J. Quant. Spectrosc. Radiative Transfer 98 (2006) 238–248.
[23] L. Chen, L. Zhang, Q. Kang, H.S. Viswanathan, J. Yao, W.Q. Tao, Nanoscale simulation of shale transport properties using the lattice Boltzmann method: permeability and diffusivity, Sci. Rep. 5 (2015).
[24] L. Chen, W. Fang, Q. Kang, J.D.H. Hyman, H.S. Viswanathan, W.Q. Tao, Generalized lattice Boltzmann model for flow through tight porous media with Klinkenberg's effect, Phys. Rev. E 91 (2015) 033004.

[25] K. Zhao, Q. Li, Y.M. Xuan, Investigation on the three-dimensional multiphase conjugate conduction problem inside porous wick with the lattice Boltzmann method, Sci. China Ser. E 52 (2009) 2973–2980.
[26] M. Wang, J. Wang, N. Pan, S. Chen, Mesoscopic predictions of the effective thermal conductivity for microscale random porous media, Phys. Rev. E 75 (2007) 036702.
[27] J. Wang, M. Wang, Z. Li, A lattice Boltzmann algorithm for fluid–solid conjugate heat transfer, Int. J. Therm. Sci. 46 (2007) 228–234.
[28] A.A. Mohamad, Lattice Boltzmann Method: Fundamentals and Engineering Applications with Computer Codes, Springer Science & Business Media, 2011.
[29] M.F. Modest, Radiative Heat Transfer, Academic Press, 2013.
[30] S.C. Mishra, H.K. Roy, N. Misra, Discrete ordinate method with a new and a simple quadrature scheme, J. Quant. Spectrosc. Radiative Transfer 101 (2006) 249–262.
[31] N. Gupta, R.C. Gorthi, S.C. Mishra, Lattice Boltzmann method applied to variable thermal conductivity conduction and radiation problems, J. Thermophys. Heat Transfer 20 (2006) 895–902.
[32] B. Mondal, S.C. Mishra, Application of the lattice Boltzmann method and the discrete ordinates method for solving transient conduction and radiation heat transfer problems, Numer. Heat Transfer A-Appl. 52 (2007) 757–775.
[33] S.C. Mishra, H. Poonia, R.R. Vernekar, A.K. Das, Lattice Boltzmann method applied to radiative transport analysis in a planar participating medium, Heat Transfer Eng. 35 (2014) 1267–1278.
[34] L. Li, C. Chen, R. Mei, J.F. Klausner, Conjugate heat and mass transfer in the lattice Boltzmann equation method, Phys. Rev. E 89 (2014) 043308.
[35] X.D. Wang, D. Sun, Y.Y. Duan, Z.J. Hu, Radiative characteristics of opacifier-loaded silica aerogel composites, J. Non-Cryst. Solids 375 (2013) 31–39.
[36] Y. Zhao, G. Tang, M. Du, Numerical study of radiative properties of nanoporous silica aerogel, Int. J. Therm. Sci. 89 (2015) 110–120.
[37] S. Zeng, A. Hunt, R. Greif, Mean free path and apparent thermal conductivity of a gas in a porous medium, J. Heat Transfer 117 (1995) 758–761.
[38] G.A. Slack, Nonmetallic crystals with high thermal conductivity, J. Phys. Chem. Solids 34 (1973) 321–335.
[39] H. Zhang, Y. Jin, W. Gu, Z.Y. Li, W.Q. Tao, A numerical study on the influence of insulating layer of the hot disk sensor on the thermal conductivity measuring accuracy, Prog. Comput. Fluid Dyn. 13 (2013) 191–201.
[40] W.Z. Fang, L. Chen, J.J. Gou, W.Q. Tao, Predictions of effective thermal conductivities for three-dimensional four-directional braided composites using the lattice Boltzmann method, Int. J. Heat Mass Transfer 92 (2016) 120–130.